



# Selective Photocatalytic Reduction of Carbon Dioxide to Carbon Monoxide by Iron and Cobalt Complexes Supported by bis-(1methyl-imidazole) diimine

Jorge Ferreira Jr, Mellanye Graf, Adriana C. A. Casagrande, Marcelo P. Gil, Osvaldo L. Casagrande Jr, \*\*

<sup>1</sup> Laboratory of Molecular Catalysis, Instituto de Química, Universidade Federal do Rio Grande do Sul, Avenida Bento Gonçalves, 9500, 90501-970, Porto Alegre, RS (Brazil).

## Resumo/Abstract

## RESUMO

Uma série de complexos de ferro(II) e cobalto(II) contendo ligantes nitrogenados tetradentados foi sintetizada e avaliada como fotocatalisadores homogêneos para a redução seletiva de CO<sub>2</sub> a CO sob irradiação de luz visível. De modo geral, os catalisadores à base de ferro e cobalto exibem atividade fotocatalítica significativa na conversão de CO<sub>2</sub> em CO, com os complexos de ferro apresentando maiores atividades e seletividade na produção de CO. Os resultados mostraram uma forte influência do tamanho da ponte alquil sobre a atividade catalítica e seletividade na produção de CO. O complexo de ferro [Fe(L1)(H<sub>2</sub>O)<sub>2</sub>(BF<sub>4</sub>)<sub>2</sub>] (Fe1), contendo uma ponte etilênica, apresentou performance catalítica superior ao Fe2, que possui uma cadeia propílica. Isso sugere que o menor impedimento estérico e um ambiente eletrônico mais favorável ao redor do centro metálico promovem melhor acesso ao substrato e desempenho catalítico superior. Notavelmente, esse efeito foi dependente do metal, já que os complexos análogos de cobalto exibiram tendências distintas. O uso de menores quantidades de Fe1 promove maior TONco (15.522) e a maior seletividade para CO (91%).

Palavras-chave: Redução de CO<sub>2</sub>, fotocatálise, complexo de ferro e cobalto, ligantes nitrogenados tetradentados

## ABSTRACT -

A series of iron(II) and cobalt(II) complexes bearing nitrogen-rich tetradentate ligands were synthesized and evaluated as homogeneous photocatalysts for the selective reduction of CO2 to CO under visible light irradiation. Overall, both iron- and cobalt-based catalysts exhibit significant photocatalytic activity for CO<sub>2</sub>-to-CO conversion, with iron complexes consistently delivering higher activities and CO selectivities. The influence of ligand architecture was evident. For instance, the iron complex [Fe(L1)(H<sub>2</sub>O)<sub>2</sub>(BF<sub>4</sub>)<sub>2</sub>] (Fe1), incorporating an ethylene-linker ligand, outperformed Fe2, which has a propylene chain. This suggests that reduced steric hindrance and a more favorable electronic environment around the metal center promote better substrate access and enhanced catalytic performance. Notably, the effect was metal-dependent, as cobalt analogues exhibited distinct trends. At lower catalyst loadings, Fe1 achieved the highest TON<sub>CO</sub> (up to 15,522) and CO selectivity (91%).

Keywords: CO<sub>2</sub> reduction, photocatalysis, iron and cobalt complexes, nitrogen tetradentate ligands

#### 1. Introduction

The rising atmospheric concentration of carbon dioxide (CO<sub>2</sub>), primarily driven by the combustion of fossil fuels and various industrial activities, represents one of the most critical environmental challenges of the 21st century. As the predominant anthropogenic greenhouse gas, CO2 plays a central role in global warming and climate change. Addressing this issue demands not only efficient strategies for CO<sub>2</sub> capture and sequestration, but also the development sustainable methodologies to convert thermodynamically stable molecule into value-added chemicals. (1-3) To date, a variety of CO<sub>2</sub> capture technologies have been developed, including chemical absorption, adsorption onto solid sorbents, and membranebased separations. While these approaches are effective in mitigating emissions at point sources, they do not eliminate the long-term problem of CO2 accumulation in the atmosphere. Consequently, the catalytic conversion of CO<sub>2</sub> into useful chemicals such as carbon monoxide (CO), formic acid, and methane has garnered increasing interest.(4-5) Among these products, CO stands out due to its role as a key feedstock in the chemical industry, especially in Fischer-Tropsch synthesis and the production of synthetic fuels.(6-7) The photocatalytic reduction of CO<sub>2</sub>



to CO, in particular, represents a promising route for CO<sub>2</sub> valorization, especially when coupled with homogeneous catalytic systems capable of utilizing solar energy—an abundant, clean, and renewable energy source.(8-10)

This transformation, however, involves complex multielectron and proton-coupled electron transfer processes, rendering catalyst design a critical factor for achieving high efficiency and selectivity. Homogeneous photocatalysts are especially appealing in this context, offering well-defined coordination environments and tunable electronic properties that can facilitate CO<sub>2</sub> activation and reduction under mild reaction conditions.

Significant research efforts have focused on transitionmetal-based homogeneous catalysts for this purpose. Complexes of ruthenium, rhodium, and iridium have shown excellent activity and selectivity; however, their high cost and low natural abundance hinder large-scale applicability. Therefore, attention has increasingly shifted toward firstrow transition metals (Fe, Mn, Co and Ni) which offer more sustainable alternatives due to their earth abundance, lower toxicity, and versatile redox behavior. In particular, iron(11-16) and cobalt(17-19) complexes bearing polydentate nitrogen-based ligands—such as bipyridine, phenanthroline, and porphyrin derivatives—have emerged as highly promising candidates for photocatalytic CO2 reduction to CO. Recent advances demonstrate that finetuning the electronic structure of metal-ligand complexes through rational ligand design can significantly enhance catalytic efficiency, selectivity, and photostability. In this paper, we highlight recent progress in the development of homogeneous iron(II) and cobalt(II) catalysts supported by bis-(1-methyl-imidazole diamine) for the photocatalytic conversion of CO<sub>2</sub> to CO. We emphasize structure-activity relationships, with a particular focus on catalytic performance under photochemical conditions, aiming to provide insight into the design principles that govern activity, selectivity, and long-term stability of these promising systems.

# 2. Experimental

#### 2.1 Materials

All solvents used in the synthesis of catalysts and photocatalytic reactions were dried over a MBraun SPS-800 purification  $Fe(BF_4)_2 \cdot 6H_2O$ , solvent system. Co(ClO<sub>4</sub>)<sub>2</sub>·6H<sub>2</sub>O and [Ru(bipy)<sub>3</sub>]Cl<sub>2</sub> were purchased from Sigma-Aldrich and used as received. BIH (1,3-dimethyl-2phenyl-2,3-dihydro-1H-benzo[d]-imidazole) was prepared according to the reported procedure.(20) Infrared spectra were performed on neat products using a FT-IR Bruker Alpha Spectrometer operating in the ATR mode. <sup>1</sup>H and <sup>13</sup>C NMR chemical shifts are reported in ppm vs. SiMe<sub>4</sub> and were determined by reference to the residual solvent peaks. Elemental analyses were performed by the Analytical Central Service of the Institute of Chemistry-UFRGS



(Brazil) and are the average of two independent determinations. High-resolution mass spectrometry (HRMS) data were collected on a Micromass Waters® Q-Tof spectrometer. CO and H<sub>2</sub> production were quantitatively assessed using a Gas Chromatograph (Agilent 7890GC) equipped with a Porapak-Q column of 80/100 mesh, a Thermal Conductivity Detector (TCD) connected in series with a Methanizer, and a Flame Ionization Detector (FID). 50 μL of gas phase samples were taken using a 100-μL gastight Hamilton sirvnge and injected in the GC in splitless mode. Calibration curves for H2 and CO were determined separately by injecting known quantities of a standard mixture (MULT MIX HC - OX - Air Liquide) containing 1,00000 % mol of hydrogen and 1,00000 % of carbon monoxide in argon.

#### 2.2 Synthesis of nitrogen tetradentate ligands

2.2.1 bis((1-methyl-4,5-dihydro-1H-imidazol-2yl)methylene)ethane-1,2-diimine. (L1). Initially, in a Schlenk under nitrogen atmosphere, sodium sulfate (3.27 g, 27.47 mmol) was added to an imidazole solution (1.501 g, 13.66 mmol) in dichloromethane (15mL). The solution was stirred for 20 minutes at room temperature. After this period, ethane-1,2-diamine (0.453mL g, 6.78 mmol) was added. The reaction was refluxed for 24 hours, and after this period, the product was washed three times with dichloromethane to be extracted and evaporated under reduced pressure, obtaining L1 as an orange solid (1.094 g, 73% yield). IR (ATR, cm<sup>-1</sup>): 3102 (w), 2942 (w), 1671 (m), 1621 (s), 1587 (s), 1472 (s), 1450 (s),1425 (s), 1405 (s), 1368 (m), 1330 (m), 1281 (m), 1224 (m), 1146 (m), 1127(m), 1106 (m), 1081 (m), 1042 (m), 918 (m), 853 (m), 737 (s). <sup>1</sup>H NMR (400 MHz, CDCl<sub>3</sub>, 25°C): δ (ppm) 8.31 (s, 2H, CH=N), 7.07 (d, 2H, Im-H), 6.90 (d,2H, Im-H), 3.94 (s, 6H, Im-CH<sub>3</sub>), 3.91 (s, 4H, CH<sub>2</sub>). Anal. Calc. for C<sub>12</sub>H<sub>16</sub>N<sub>6</sub>: C: 59.00, H: 6.60, N: 34.40. Found: C: 58.86, H: 6.19, N: 34.03. HRMS (ESI<sup>+</sup>): exact mass calculated for [M+H]<sup>+</sup> (C<sub>12</sub>H<sub>17</sub>N<sub>6</sub>) requires m/z 245.1515, found: m/z 245.1509.

2.2.2 bis((1-methyl-1H-imidazol-2-yl)methylene)propane-1,3-diimine (**L2**). This ligand was was prepared as described above for **L1**, starting from propane-1,3-diamine (1.156 g, 15.6 mmol) and imidazole solution (3.435 g, 31.2 mmol) in dichloromethane (15mL) give **L2** as an orange solid (2.147 g, 54 % yield). <sup>1</sup>H NMR (400 MHz, CDCl<sub>3</sub>, 25°C):  $\delta$  (ppm) 8.33 (s, 2H, C*H*=N), 7.09 (d, 2H, Im-H), 6.91 (d,2H, Im-H), 3.98 (s, 6H, Im-CH<sub>3</sub>), 3.68 (s, 4H, CH<sub>2</sub>CH<sub>2</sub>CH<sub>2</sub>), 2.03 (s, 2H, CH<sub>2</sub>CH<sub>2</sub>CH<sub>2</sub>). Anal. Calc. for C<sub>13</sub>H<sub>18</sub>N<sub>6</sub>: C: 60.44, H: 7.02, N: 32.53. Found: C: 59.24, H: 7.64, N: 32.04. HRMS (ESI<sup>+</sup>): exact mass calculated for [M+H]<sup>+</sup> (C<sub>13</sub>H<sub>19</sub>N<sub>6</sub>) requires m/z 259.1671, found: m/z 259.1669.

## 2.3 Synthesis of iron and cobalt complexes

2.3.1 [Fe(L1)( $H_2O$ )<sub>2</sub>](BF<sub>4</sub>)<sub>2</sub> (Fe1). Fe(BF<sub>4</sub>)<sub>2</sub>·6H<sub>2</sub>O (0.1359 g, 0.4.027 mmol) and L1 (0.1009 g, 0.4.027 mmol) in degassed acetonitrile (10 mL) was stirred under nitrogen



under for 24 h at 25°C. The purple solid was filtered off, washed with diethyl ether (3 x 5mL) and dried under vacuum. (0.1437 g, 72% yield). Anal. Calc. for  $C_{12}H_{20}B_2F_8FeN_6O_2$ : C: 27.58, H: 4.04, N: 15.24. Found: C: 28.27, H: 3.95, N: 16.49. HRMS (ESI<sup>+</sup>): exact mass calculated for [M-(BF<sub>4</sub>)<sub>2</sub>-2H<sub>2</sub>O-H]<sup>2+</sup> ( $C_{12}H_{15}FeN_6$ ) requires m/z 299.0708, found: m/z 299.0702.

2.3.2 [Fe(L2)(H<sub>2</sub>O)<sub>2</sub>](BF<sub>4</sub>)<sub>2</sub> (**Fe2**). Fe(BF<sub>4</sub>)<sub>2</sub>·6H<sub>2</sub>O (0.1307 g, 0.3871 mmol) and **L2** (0.1000 g, 0.3871 mmol) in degassed acetonitrile (10 mL) was stirred under nitrogen under for 24 h at 25°C. The purple solid was filtered off, washed with diethyl ether (3 x 5mL) and dried under vacuum. Yield: 0.1590 g (85%). Anal. Calc. for  $C_{13}H_{22}B_2F_8FeN_6O_2$ : C: 29.81, H: 4.23, N: 16.04. Found: C: 29.73, H: 4.07, N: 15.91.

2.3.3  $[Co(L2)(H_2O)_2](ClO_4)_2$  (Co1).  $Co(ClO_4)_2 \cdot 6H_2O$  6H2O (0.1474 g, 0.4027 mmol) and L1 (0.1000 g, 0.4027 mmol) in degassed acetonitrile (10 mL) was stirred under nitrogen under for 24 h at 25°C. The beige solid was filtered off, washed with diethyl ether (3 x 5mL) and dried under vacuum. Yield: 0.1739 g (80%).Anal. Calc. for  $C_{12}H_{20}Cl_2F_8CoN_6O_{10}$ : C: 26.78, H: 3.75, N: 15.62. Found: C: 26.27, H: 3.85, N: 15.06. HRMS (ESI<sup>+</sup>): exact mass calculated for [M-(ClO<sub>4</sub>)<sub>2</sub>-2H<sub>2</sub>O]<sup>2+</sup> ( $C_{12}H_{16}CoN_6$ ) requires m/z 151.5384, found: m/z 151.5378.

2.3.4 [Co(L2)(H<sub>2</sub>O)<sub>2</sub>](ClO<sub>4</sub>)<sub>2</sub> (**Co2**). This complex was prepared as described above for **Co1**, starting from L2 (0.100 g, 0.3871 mmol) and Co(ClO<sub>4</sub>)<sub>2</sub>·6H<sub>2</sub>O (0.14165 g, 0.3871 mmol) in acetonitrile (10 mL) to give **Co2** as an orange solid (0.1661 g, 78% yield). Anal. Calc. for  $C_{13}H_{22}Cl_2F_8CoN_6O_{10}$ : C: 28.28, H: 4.02, N: 15.22. Found: C: 27.89, H: 3.97, N: 14.98. HRMS (ESI<sup>+</sup>): exact mass calculated for [M-(ClO<sub>4</sub>)<sub>2</sub>-2H<sub>2</sub>O]<sup>2+</sup> ( $C_{13}H_{18}CoN_6$ ) requires m/z 158.6311, found: m/z 158.5457.

#### 2.4 Photocatalytic CO<sub>2</sub> reduction

Photocatalytic  $CO_2$  reduction was performed in a borosilicate photoreactor designed in our group (volume = 12.0 mL) containing a solution of the catalyst (50.0  $\mu$ M),  $[Ru(bipy)_3]^{2+}$  (0.3 mM) and BIH (0.11 M) in a  $CO_2$ -saturated MeCN/H<sub>2</sub>O solution (4.0 mL). The photoreactor was sealed with a rubber septum and then purged with  $CO_2$  for 20 mins. The photoreactor was placed inside the illumination chamber equipped with LED strip (blue light,  $\lambda = 460$  nm) with light irradiance 403  $\mu$ W·cm<sup>2</sup>nm<sup>-1</sup>. The distance of the reactor external wall to the light source was 5 cm.

# 3. Results and Discussion

## 3.1 Synthesis and Characterization of iron complexes

The bis(1-methyl-imidazole diimine) ligands **L1** and **L2** were synthesized via Schiff base condensation between 1-methyl-2-imidazolecarboxaldehyde and the respective diamine. These ligands were obtained as orange solids in moderate to good yields (73 and 54 %, respectively), and



characterized by elemental analysis, IR spectroscopy, ESI-HRMS and  $^{1}H$  and  $^{13}C\{^{1}H\}$  NMR. The reaction of **L1-L2** with 1 equiv of Fe(BF<sub>4</sub>)<sub>2</sub>·6H<sub>2</sub>O or Co(ClO<sub>4</sub>)<sub>2</sub>·6H<sub>2</sub>O in CH<sub>3</sub>CN at room temperature yielded the corresponding iron (**Fe1-Fe2**) and cobalt (**Co1-Co2**) complexes which were isolated in good to excellent yields (72–85%) (Scheme 1). These complexes were characterized by elemental analysis and ESI-HRMS. Elemental analysis confirmed the formation of the desired iron and cobalt complexes, supporting a formulation of [M(L)(H<sub>2</sub>O)<sub>2</sub>]X<sub>2</sub> (M = Fe, Co; X = BF<sub>4</sub>, ClO<sub>4</sub>), consistent with the coordination of two water molecules.

**Scheme 1**. Synthesis of iron(II) and Co(II) complexes.

## 3.2 Photocatalytic studies

The catalytic performance of iron (Fe1-Fe2) and cobalt complexes (Co1-Co2) was evaluated under identical reaction conditions as presented in the Experimental section. The gas products (CO and  $H_2$ ) were quantified by headspace gas chromatography analysis, while the formation of formate was monitored by  $^1H$  NMR spectroscopy. No significant amounts of formate or CH4 were detected. Control experiments conducted in the absence of a catalyst or using Fe(BF4)2 and Co(ClO4)2 as catalysts resulted in only small amounts of CO and  $H_2$ . These baseline results underscore the essential role of the iron/cobalt complexes in photocatalysis, demonstrating that coordination of the ligand to the metal center is crucial for achieving high turnover numbers and enhanced selectivity for CO production.

Overall, both iron- and cobalt-based catalysts exhibit significant photocatalytic activity for CO<sub>2</sub>-to-CO conversion, with iron complexes consistently delivering higher turnover numbers and selectivity under comparable conditions as presented in Figure 1. The TOF<sub>CO</sub> values for **Fe1/Fe2** and **Co1/Co2** range from 46.5 to 61.8 h<sup>-1</sup>, with **Co2** achieving the highest turnover frequency. Notably, a clear trend is observed for **Fe1**, where lower catalyst concentrations lead to increased TOF<sub>CO</sub> values reaching 646.7 h<sup>-1</sup>, highlighting the significant impact of catalyst loading on photocatalytic performance.



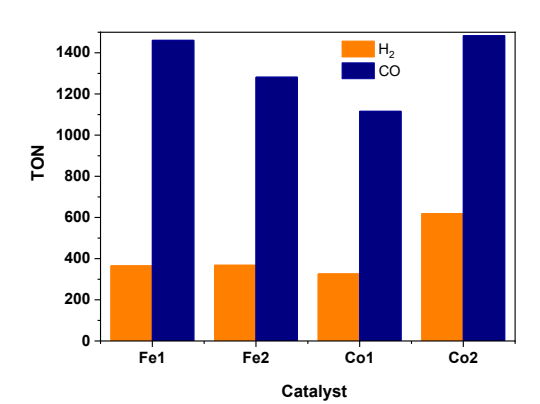


**Figure 1.** TON for photocatalytic CO<sub>2</sub>-to-CO conversion by various iron catalysts in aqueous CH<sub>3</sub>CN (7.5 % H<sub>2</sub>O).

Among the iron-based catalysts, Fe1 and Fe2, the primary difference lies in the alkyl chain length (ethyl and propyl).



**Fe1** bearing an ethylenic bridge exhibits a higher turnover number for CO production ( $TON_{CO} = 1461$ ) and selectivity towards CO ( $Sel_{CO} = 80.0\%$ ) compared to **Fe2** ( $TON_{CO} = 1282$ ;  $Sel_{CO} = 73.5\%$ ). This suggests that a shorter ethyl substituent may promote a more favorable electronic or steric environment for  $CO_2$  activation and reduction. The slightly increased steric hindrance introduced by the propyl unit in **Fe2** might hamper optimal catalyst-substrate interactions or influence the binding mode of  $CO_2$  at the active site, thus reducing overall efficiency and selectivity.

An opposite trend was observed within the cobalt series. **Co1** delivers a lower TON<sub>CO</sub> (1116) and CO selectivity (77.4%) than **Co2**, which reaches a TON<sub>CO</sub> of 1483 and a Sel<sub>CO</sub> of 70.6%. This contrasting behavior related to the iron complexes suggests that the impact of alkyl chain length is metal-dependent and may be related to differences in coordination geometry, electronic configuration, or ligand field effects intrinsic to each metal center.

Table 1. Visible-light-drive catalytic reduction of CO<sub>2</sub> by iron and cobalt complexes.<sup>a</sup>

		Time	H <sub>2</sub> O	TON		[H]	[CO]	Sel. CO	TOF
Entry	Catalyst	(h)	(%)	(H <sub>2</sub> )	(CO)	(µmol)	(µmol)	(%)*	(h <sup>-1</sup> )
$1^b$	-	24	7.5	14	61	16.8	73.2	81.0	2.54
2	Fe1	24	7.5	365	1461	73.0	292.4	80.0	<mark>60.9</mark>
3	Fe2	24	7.5	368	1282	73.5	256.3	73.5	53.4
4	Co1	24	7.5	326	1116	65.2	223.2	77.4	46.5
5	Co2	24	7.5	619	1483	123.7	296.6	70.6	61.8
6 <sup>c</sup>	Fe1	24	7.5	402	2805	44.1	313.0	87.6	116.9
$7^d$	Fe1	24	7.5	880	4334	44.0	216.7	83.1	180.6
8 <sup>e</sup>	Fe1	24	7.5	1253	13529	31.32	338.2	91.5	563.7
9 <sup>f</sup>	Fe1	24	7.5	1533	15522	19.2	194.0	91.0	<mark>646.7</mark>

a Reaction conditions unless specified otherwise:  $50.0~\mu M$  catalyst, 0.3~m M [Ru(bipy)<sub>3</sub>]<sup>2+</sup> and 0.11~M BIH, 24~h in a CO<sub>2</sub>-saturated MeCN/H<sub>2</sub>O solution (4 mL) at 308 K upon visible light irradiation (460 nm). <sup>b</sup> Without catalyst. <sup>c</sup> using catalyst concentration of  $25.0~\mu M$ , <sup>d</sup> using catalyst concentration of  $25.0~\mu M$ , <sup>e</sup> using catalyst concentration of  $25.0~\mu M$ , <sup>e</sup> using catalyst concentration of  $25.0~\mu M$ , <sup>e</sup> using catalyst concentration of  $25.0~\mu M$ , f using catalyst concentration of  $25.0~\mu M$ , All experiments were performed at least two times, having good reproducibility (error 25-10%). \* Selco = [mmol(CO)/(mmol(H<sub>2</sub>)+mmol(CO)]x100.

Comparing across metal centers, Fe1 outperforms Co1 in both CO production and selectivity, highlighting the superior activity of iron under these reaction conditions when using the ethyl-substituted ligand. Interestingly, although Co2 surpasses Co1 in CO productivity, its

selectivity is lower than that of Fe1, reinforcing the notion that iron complexes, particularly with smaller alkyl substituents, offer a more favorable balance between activity and selectivity for photocatalytic  $CO_2$ -to-CO conversion. These findings emphasize the dual importance



of metal identity and ligand architecture in tuning the photocatalytic performance of homogeneous systems.

In general, the results indicate that both the ligand alkyl chain and the metal center play critical roles in modulating the catalyst performance. The shorter ethyl group enhances selectivity and efficiency in Fe-based systems, likely through improved substrate accessibility and favorable orbital interactions, while Co-based systems respond differently, suggesting that the optimization of such homogeneous photocatalysts must account for metal-specific electronic and steric considerations.

In order to evaluate the influence of concentration of catalyst reaction on the TON and selectivity, a series of photocatalytic reactions were performed using Fe1 (Figure 2). A systematic variation of the Fe1 catalyst concentration reveals a clear inverse correlation between catalyst loading and both the TON<sub>CO</sub>) and selectivity toward CO production. As the concentration of Fe1 is decreased from 50.0  $\mu$ M to 3.12  $\mu$ M, a substantial increase in TON<sub>CO</sub> is observed, from 1,461 to 15,522, indicating a more efficient utilization of catalytic sites at lower concentrations.

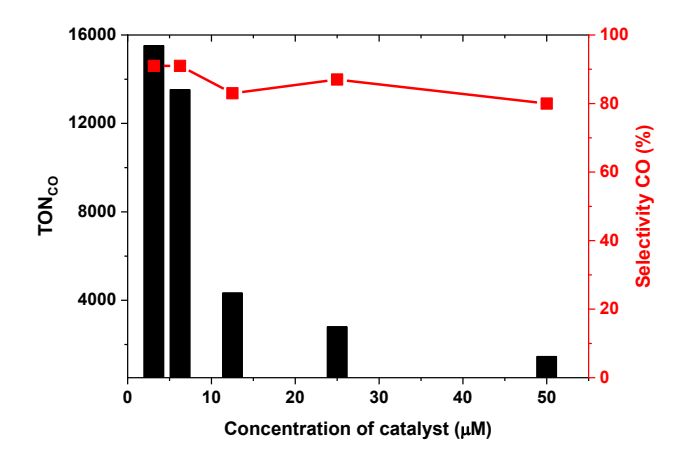


Figure 2. Concentration dependence of Fe1 on  $TON_{CO}$  and selectivity.

This trend can be rationalized by considering both kinetic and photophysical factors. At higher catalyst concentrations, a larger proportion of the Fe1 molecules may remain unproductive, either due to limited light penetration (inner filter effect) or to aggregation or self-quenching phenomena that reduce the effective concentration of photoactive species. Conversely, at lower catalyst concentrations, light absorption becomes more uniform throughout the solution, and each Fe center has a higher probability of participating in the catalytic cycle, leading to significantly enhanced turnover numbers.

Notably, the CO selectivity also improves as the catalyst concentration decreases. At 50.0  $\mu$ M, Sel<sub>CO</sub> is 80.0%, increasing steadily to 91.0% at 3.12  $\mu$ M. This enhancement



may be attributed to a shift in the competitive kinetics of  ${\rm CO_2}$  reduction versus proton reduction. At lower catalyst concentrations, the local concentration of active Fe species may favor  ${\rm CO_2}$  activation pathways over hydrogen evolution, potentially due to reduced metal-metal interactions or changes in intermediate speciation. Furthermore, at diluted conditions, the reaction environment may more strongly favor single-site catalysis, minimizing side reactions that lead to  ${\rm H_2}$  formation

The intermediate data points reinforce this trend: at  $6.25~\mu M$ ,  $TON_{CO}$  already reaches 13529 with a high CO selectivity of 91.5%. These results highlight the importance of optimizing catalyst loading to balance photon absorption, catalytic efficiency, and product selectivity. Thus, these findings underscore that lower **Fe1** catalyst concentrations not only enhance catalytic efficiency as quantified by  $TON_{CO}$  but also improve product selectivity, providing valuable insights for the rational design and deployment of homogeneous photocatalytic systems for selective  $CO_2$ -to-CO conversion.

Based on the photocatalytic results a plausible mechanism is presented in Figure 3.

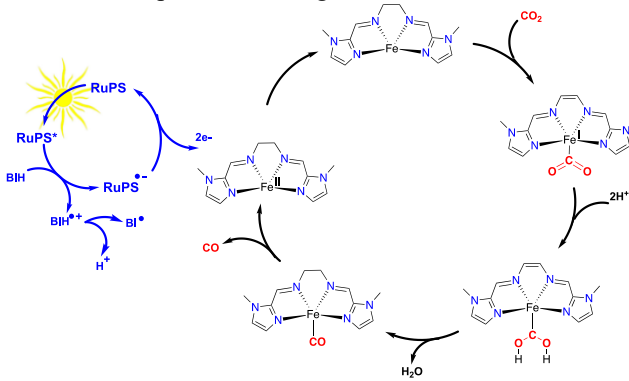


**Figure 3.** Proposed reaction mechanism for photochemical CO2 reduction using Fe1 catalyst.

The proposed photocatalytic mechanism for CO<sub>2</sub> reduction with the Fe1 complex involves a two-electron transfer from the photosensitizer [Ru(bpy)<sub>3</sub>]<sup>2+</sup>, which operates through a reductive quenching cycle under visible light irradiation. Upon photoexcitation, [Ru(bpy)<sub>3</sub>]<sup>2+</sup> is reductively quenched by the sacrificial electron donor BIH, forming the reduced [Ru(bpy)3] species. A second reduction step, also mediated by BIH, generates [Ru(bpy)<sub>3</sub>]<sup>0</sup>, a potent two-electron donor. This fully reduced photosensitizer then transfers two electrons sequentially or concertedly to the Fe(II) complex, yielding a Fe<sup>0</sup> or a formally Fe(I) intermediate capable of binding and activating CO<sub>2</sub>. Coordination of CO<sub>2</sub> to the electron-rich Fe center facilitates nucleophilic attack on the electrophilic carbon of CO2, forming a Fe-CO2 adduct. Proton-coupled electron transfer (PCET) steps then convert this



intermediate into a Fe–COOH species. A second protonation step cleaves the C–O bond, releasing CO and regenerating the initial Fe(II) state, thus closing the catalytic cycle. The ability of the Fe complex to accept two electrons and undergo reversible redox cycling is crucial for enabling the multielectron reduction of CO<sub>2</sub>. This mechanism also helps rationalize the high selectivity for CO over H<sub>2</sub>, as the reduced iron intermediate preferentially activates CO<sub>2</sub> rather than protons under the applied conditions.

# 4. Conclusion

In summary, we have developed and characterized a new family of iron(II) and cobalt(II) complexes supported by bis-(1-methyl-imidazole diimine) ligands, and use of them as homogeneous photocatalysts for the selective reduction of carbon dioxide to carbon monoxide under visible light irradiation. Among the investigated catalytic systems, Fe1 incorporating a short ethylene-bridged ligand, consistently exhibited superior catalytic performance in terms of turnover number and product selectivity when compared to its propylene analogue Fe2. This highlights the critical role of ligand design, where subtle changes in the alkyl chain length can significantly influence the electronic environment and steric accessibility of the active site, thereby modulating CO<sub>2</sub> activation pathways and catalytic efficiency. On the other hand, the higher catalytic performance of Co2 (propyl substituent) related to Co1, suggests that the impact of alkyl chain length is metaldependent and may be related to differences in coordination geometry, electronic configuration, or ligand field effects intrinsic to each metal center. Fe1 showed a strong dependence on catalyst concentration. As the catalyst loading decreased, the turnover number increased dramatically reaching up to 15522 accompanied by improved CO selectivity of up to 91%. These results can be attributed to reduced inner filter effects, minimized selfquenching, and enhanced photonic utilization at lower concentrations. Such findings reinforce the importance of optimizing not only the molecular structure of the catalyst but also the reaction conditions to maximize performance. Taken together, the results of this study offer valuable design principles for advancing the development of sustainable, earth-abundant metal-based photocatalysts for CO<sub>2</sub> valorization. The promising performance of Fe1 under low loading concentration positions it as a highly attractive candidate for further investigation in scalable artificial photosynthesis and carbon recycling technologies.

## 5. Acknowledgments

The authors are gratefully acknowledged by RITE-FAPERGS (Grant/Award Number: 22/2551-0000386-9) for the financial support.



#### 6. References

- 1. Nocera, D. G. Acc. Chem. Res. 2017, 50, 616-619.
- 2. Takeda, H.; Cometto, C.; Ishitani, O.; Robert, M. *ACS Catal.* **2017**, *7*, 70–88.
- 3. Pannwitz, A.; Klein, D. M.; Rodríguez-Jiménez, S.; Casadevall, C.; Song, H.; Reisner, E.; Hammarström, L.; Bonnet, S. *Chem. Soc. Rev.* **2021**, *50*, 4833–4855.
- 4. Appel, A. M.; Bercaw, J. E.; Bocarsly, A. B.; Dobbek, H.; DuBois, D. L.; Dupuis, M.; Fujita, E.; P. J. A.; Morris, R. H.; Peden, C. H. F.; Portis, A. R.; Ragsdale, S. W.; Rauchfuss, T. B.; Reek, J. N. H.; Seefeldt, L. C.; Thauer, R. K.; Waldrop, G. L. *Chem. Rev.* **2013**, *113*, 6621–6658.
- Tang, B.; Xiao, F.-X. ACS Catal. 2022, 12, 9023–9057.
  Kunene, T.; Xiong, L.; Rosenthal, J. Proc. Natl. Acad. Sci.
- 6. Kunene, T.; Xiong, L.; Rosenthal, J. Proc. *Natl. Acad. Sci. U. S. A.* **2019**, *116*, 9693–9695.
- 7. Rosenthal, J. In Prog. Inorg. Chem., Karlin, K. D., Ed.; Wiley: Hoboken, NJ, **2014**, 59, 40.
- 8. Masdeu-Bultó, A. M.; Reguero, M.; Claver, C., *Eur. J. Inorg. Chem.* **2022**, e202100975.
- 9. Dalle, K. E.; Warnan, J.; Leung, J. J.; Reuillard, B.; Karmel, I. S.; Reisner, E. *Chem. Rev.* **2019**, *119*, 2752–2875.
- 10. Ma, F.; Luo, Z.-M.; Wang, J.-W.; Aramburu-Trŏselj, B. M.; Ouyang, G. *Coord. Chem. Rev.* **2024**, *500*, 215529.
- 11. Guo, Z.; Cheng, S.; Cometto, C.; Anxolabéhère-Mallart, E.; Ng, S.-M.; Ko, C.- C.; Liu, G.; Chen, L.; Robert, M.; Lau, T.-C., *J. Am. Chem. Soc.* **2016**, *138*, 9413–9416.
- 12. Wang, Y.; Liu, T.; Chen, L.; Chao, D. *Inorg. Chem.* **2021**, *60*, 5590–5597.
- 13. E. A. Mohamed, Z. N. Zahran and Y. Naruta, *Chem. Commun.*, **2015**, *51*, 16900.
- 14. S. Sinha and J. J. Warren, *Inorg. Chem.*, **2018**, *57*, 12650.
- 15. S. Fukuzumi, Y.-M. Lee, H. S. Ahn and W. Nam, Chem. Sci., **2018**, *9*, 6017.
- 16. A. Ogawa, K. Oohora, W. Gua and T. Hayashi, Chem. Commun., **2018**, *55*, 493.
- 17. Zhang, X.; Yamauchi, K.; Sakai, K. ACS Catal. **2021**, 11, 10436–10449.
- 18. Boudreaux, C. M.; Nugegoda, D.; Yao, W.; Le, N.; Frey, N. C.; Li, Q.; Qu, F.; Zeller, M.; Webster, C. E.; Delcamp, J. H.; Papish, E. T., ACS Catal. **2022**, *12*, 8718–8728.
- 19. Ho, P.-Y.; Cheng, S.-C.; Yu, F.; Yeung, Y.- Y.; Ni, W.-X.; Ko, C.-C.; Leung, C. F.; Lau, T.-C.; Robert, M. ACS Catal. **2023**, *13*, 5979–5985.
- 20. Sampaio, R. N.; Grills, D. C.; Polyansky, D. E.; Szalda, D. J.; Fujita, E. *J. Am. Chem. Soc.* **2020**, *142*, 2413–2428.